Model of plastic deformation for extreme loading conditions

Dean L. Preston, Davis L. Tonks, and Duane C. Wallace

Additional information on J. Appl. Phys.

Model of plastic deformation for extreme loading conditions

Dean L. Preston[a] and Davis L. Tonks[b]
Applied Physics Division, Los Alamos National Laboratory, Los Alamos, New Mexico 87545

Duane C. Wallace
Applied Physics Division and Theoretical Division, Los Alamos National Laboratory, Los Alamos, New Mexico 87545

We present a model of metallic plastic flow suitable for numerical simulations of explosive loading and high velocity impacts. The dependence of the plastic strain rate on applied stress at low strain rates is of the Arrhenius form but with an activation energy that is singular at zero stress so that the deformation rate vanishes in that limit. Work hardening is modeled as a generalized Voce law. At strain rates exceeding 10^9 s^{-1}, work hardening is neglected, and the rate dependence of the flow stress is calculated using Wallace's theory of overdriven shocks in metals [D.C. Wallace, Phys. Rev. B **24**, 5597 (1981); **24**, 5607 (1981)]. The thermal-activation regime is continuously merged into the strong shock limit, yielding a model applicable over the 15 decades in strain rate from 10^{-3} to 10^{12} s^{-1}. The model represents all aspects of constitutive behavior seen in Hopkinson bar and low-rate data, including a rapid increase in the constant-strain rate sensitivity, with 10% accuracy. High-pressure behavior is controlled by the shear modulus, $G(\rho,T)$, and the melting temperature, $T_m(\rho)$. There are eleven material parameters in addition to $G(\rho,T)$ and $T_m(\rho)$. Parameters for Cu, U, Ta, Mo, V, Be, 304 SS, and 21-6-9 SS are provided. © *2003 American Institute of Physics.* [DOI: 10.1063/1.1524706]

I. INTRODUCTION

Numerical simulations of metals and alloys during explosively driven deformation and high-velocity impacts require a physically realistic model of plastic constitutive behavior. The main difficulty in constructing such a model is the wide range of mechanical and thermodynamic conditions that can occur in solid flow processes of interest: plastic strains of several hundred percent, plastic strain rates up to 10^{11} s^{-1} (hypervelocity impacts), pressures exceeding 10 GPa, and temperatures up to melt. Others have developed a number of models, each emphasizing one or two aspects of material response, but being otherwise deficient.[1,2] In particular, plastic constitutive models based on thermally activated dislocation glide alone are restricted in applications to strain rates $\leqslant 10^5$ s^{-1}. In contrast, the model discussed in this article is applicable at strain rates spanning the range $10^{-3}-10^{12}$ s^{-1}. This was achieved by merging the flow properties of metals in the strong-shock-wave limit, where nonlinear dislocation drag effects are expected to predominate, with the thermal-activation regime. A second feature of this model is that it is a scaled variable, i.e., dimensionless, formulation. The flow stress and temperature are scaled by the shear modulus and melting temperature, respectively, hence the complete constitutive model includes melt curves and a density- and temperature-dependent model for the shear modulus. This constitutive model provides unprec-

edented predictive capability under the extreme conditions characteristic of high-velocity impacts and explosive deformations.

The plastic constitutive relation presented here is a physically based model; that is, it is a mathematical representation of solid flow with parameters related to known physical processes. This implies that, in the absence of experimental data, one can still obtain an approximate description of the material response by estimating the physical parameters involved. We find, for example, that metals in the same crystal class have parameters tightly clustered around a central value.

II. BASIC ASSUMPTIONS

The dynamic response of a material depends only on its current microstructural state, which is characterized by its grain size distribution, the distribution of grain orientations, dislocation density, dislocation network structure, volume fraction of twins, etc. A plastic constitutive relation depends in general on the complete set of internal state variables that represent the microstructural state, although of course the dependence on some of those variables may be relatively weak. The ideal continuum model employs true internal state variables, is constructed using a sophisticated homogenization procedure relating the internal state to the continuum response, includes a model for microstructure evolution, and requires complete microstructure characterization for its utilization. This achievement is certainly many years in the future. A step in this direction has been taken by Follansbee and Kocks[3] who developed a constitutive model employing the mechanical threshold stress (flow stress at 0 K) as a

[a]Electronic mail: dean@lanl.gov
[b]Electronic mail: tonks@lanl.gov

structure parameter, but because it accounts only for thermally activated dislocation motion, it cannot be reliably extended to strain rates much above 10^4 s^{-1}. Recognizing current theoretical and experimental limitations, we use the equivalent plastic strain ψ (often denoted ε) as an *approximate* internal state variable. This approximation, which is tantamount to neglecting path dependence, is accurate at Hopkinson bar strain rates to 10% in the stress, as seen from rate-jump tests.[3,4]

We neglect material anisotropy at all length scales. Hence, the shear elastic response and dislocation properties, in general dependent on single-crystal elastic constants, are described by the shear modulus alone. In addition, macroscopic texturing (grain alignment) is not taken into account. The equivalent plastic strain is the only structure parameter appearing in our model.

Any physically based model of constitutive behavior, or a model of any physical system for that matter, must be scale invariant, that is, invariant under arbitrary changes in the system of units. Scale invariance underlies the modern method of dimensional analysis, which can be used to model very complex systems. An understanding of the physics leads to the identification of the most important dimensional system variables which are then combined, often by simply forming ratios, into several dimensionless variables $x_1, x_2, \ldots, x_n$. The system is then described by a scale-invariant equation $f(x_1, x_2, \ldots, x_n) = 0$. Dimensional analysis does not give the function f, but f can be determined by experimental data. The result is a model of the system. This is precisely the course that we have followed to construct the model presented here.

III. MODEL VARIABLES

We denote the flow stress, the stress required to plastically deform the metal or alloy, by τ, which is one-half the von Mises equivalent deviatoric stress σ. The differential plastic work is $2\tau d\psi$.

Our constitutive relation involves three dimensionless variables. Consider first the flow stress. Since the work of Taylor in 1934 (Ref. 5) it has been known that dislocations are responsible for plastic flow. In an isotropic solid, the elastic stress field and the energy per unit length of a dislocation, as well as the long range forces between dislocations, are proportional to the shear modulus G; if G were zero there would be no dislocations and no plastic flow. It is reasonable to assume that the flow stress is likewise proportional, at least approximately, to the shear modulus. Thus, the dimensionless stress variable in our model is $\hat{\tau} = \tau/G(\rho, T)$, where ρ is the mass density and T is the temperature.

The choice of temperature scale is less obvious. One possibility is the Debye temperature θ_D of the solid. However, in a real (crystalline) solid, different measured properties yield different effective Debye temperatures, and furthermore, Debye temperatures so determined are temperature dependent. A second, and preferable, choice for the temperature scale is the melting temperature T_m. Either the Lindemann melting criterion[6] or the Burakovsky–Preston melting relation[7] relates T_m to θ_D. It is a good approximation for

most metals to drop the longitudinal sound contribution to θ_D with the result:

$$k_B \theta_D \approx \frac{h}{2\pi} \left(\frac{9\pi^2 \rho}{M} \right)^{1/3} \left(\frac{G}{\rho} \right)^{1/2}, \tag{1}$$

where M is the atomic mass. The Burakovsky–Preston melting relation tells us that $T_m \propto G$, hence $T_m \propto \theta_D^2$, which also follows from the Lindemann criterion. Therefore, T_m and θ_D are not independent choices for the temperature scale. We have chosen the scaled temperature variable in our model to be $\hat{T} = T/T_m(\rho)$.

A natural time scale for any crystalline solid is the atomic vibration time, or equivalently the Debye frequency $\omega_D = 2\pi k_B \theta_D / h$. Using the approximation of Eq. (1) we have

$$\frac{\omega_D}{3\sqrt{\pi}} \approx \frac{1}{2} \left(\frac{4\pi\rho}{3M} \right)^{1/3} \left(\frac{G}{\rho} \right)^{1/2} = \frac{c_T}{2a} \equiv \dot{\xi}, \tag{2}$$

where c_T is the transverse sound speed, and $4\pi a^3/3$ is the atomic volume. Hence, $\dot{\xi}^{-1}$ is the time required for a transverse wave to cross an atom. ω_D and $\dot{\xi}$ are equivalent scaling factors. The dimensionless strain-rate variable in our model is $\dot{\psi}/\dot{\xi}$.

IV. THERMALLY ACTIVATED DISLOCATION GLIDE

At strain rates up to at least 10^4 s^{-1} the strain rate controlling mechanism is the thermally activated interaction of dislocations with obstacles, usually other dislocations. Applied stress fields result in differential dislocation motion and dislocation intersection. For sufficiently low applied stresses the intersecting dislocations do not immediately pass through one another because of short distance repulsion (energy barrier), but thermal fluctuations can eventually drive the more mobile dislocation through its partner. The thermally assisted transition rate is given by transition state theory,[8] which is based on the assumptions that (1) the dislocations live in local minima of the crystal potential biased by the applied stress, (2) the minima are separated by a single saddle point, and (3) thermal equilibrium is maintained throughout the transition process. It follows that the dislocation transition rate, and therefore the plastic strain rate, is of the Arrhenius form

$$\dot{\psi} = \dot{\psi}_0 \exp[-\Delta\Phi(\tau)/k_B T], \tag{3}$$

where the activation energy $\Delta\Phi(\tau)$, a decreasing function of the applied stress, is the difference in the biased crystal potential between the saddle point and the initial minimum, and $\dot{\psi}_0$ is proportional to the dislocation vibration frequency in the direction of the saddle point. The simplest choice for the activation energy is $\Delta\Phi(\tau) = \Delta\Phi(0) - \nu_A \tau$ with ν_A an activation volume. Most models of plastic constitutive behavior are based on this simple Arrhenius form. It is important, however, for the purpose of model building to understand its limitations and rectify them. Equation (3) is satisfied only if the potential barrier is large compared to the thermal energy $k_B T$, that is $\Delta\Phi/k_B T \gg 1$. As the stress is increased, $\Delta\Phi/k_B T$ approaches zero and the Arrhenius form (3) for the strain rate

becomes less accurate. However, thermal activation is no longer rate controlling at high stresses, but instead dislocation drag mechanisms are expected to predominate. In our model we incorporate this transition in rate controlling mechanism by joining the Arrhenius form onto a power-law dependence at very high strain rates. In addition to its large-τ breakdown, the Arrhenius form gives an unphysical finite strain rate at zero τ. This failure occurs because it does not account for backward motion through the saddle point when the bias is removed; the reverse flow is exponentially suppressed at finite stress. In the present model this deficiency is eliminated by introducing a singular $\Delta\Phi$, specifically the inverse error function.

The Arrhenius equation, Eq. (3) shows that the stress is a function of the variable $k_B T \ln(\dot{\psi}_0/\dot{\psi})$. This form suggests the analogous combination $\kappa \hat{T} \ln(\gamma \dot{\xi}/\dot{\psi})$ for our model; κ and γ are dimensionless material constants.

The work hardening saturation stress and yield stress in the thermal activation regime are given by

$$\hat{\tau}_s = s_0 - (s_0 - s_\infty)\text{erf}[\kappa \hat{T} \ln(\gamma \dot{\xi}/\dot{\psi})],$$
$$\hat{\tau}_y = y_0 - (y_0 - y_\infty)\text{erf}[\kappa \hat{T} \ln(\gamma \dot{\xi}/\dot{\psi})]. \tag{4}$$

Each can be written in the Arrhenius form with $\Delta\Phi(\hat{\tau}_c) \sim \text{erf}^{-1}[(c_0 - \hat{\tau}_c)/(c_0 - c_\infty)]$ where $c = s$ or y. The material constants s_0 and s_∞ are the values that $\hat{\tau}_s$ takes at zero temperature and very high temperature, respectively; y_0 and y_∞ have analogous interpretations. The error function was chosen because it changes abruptly from nearly linear for $x \lesssim 1$ to a constant for $x \gtrsim 1$. The same behavior cannot be obtained with rational functions unless additional material constants are introduced. This abrupt transition is evident in the data, particularly in the bcc metals. Figure 1 is a plot of tantalum yield stress data as a function of (a) T and (b) $\hat{T} \ln(\gamma \dot{\xi}/\dot{\psi})$. The widely scattered data in (a) dramatically collapse to a single curve in (b) that is fit very well by our model expression for $\hat{\tau}_y$ employing the error function.

Our work hardening law is an extension of the well-known Voce behavior,[9] that is, a linear decrease in the work hardening rate as $\tau \to \tau_s$:

$$\frac{d\hat{\tau}}{d\varepsilon} = \theta \frac{\hat{\tau}_s - \hat{\tau}}{\hat{\tau}_s - \hat{\tau}_y} \quad \text{(Voce)}. \tag{5}$$

A constant initial work hardening rate is observed in both fcc and bcc metals, in agreement with Eq. (5). Our extension of Eq. (5) was motivated by the additional observation that the work hardening rate in fcc metals decreases less rapidly to zero as the saturation stress increases. Such behavior is captured by the following expression for the work hardening rate

$$\frac{d\hat{\tau}}{d\varepsilon} = \theta \frac{\exp\left[p\dfrac{\hat{\tau}_s - \hat{\tau}}{s_0 - \hat{\tau}_y}\right] - 1}{\exp\left[p\dfrac{\hat{\tau}_s - \hat{\tau}_y}{s_0 - \hat{\tau}_y}\right] - 1}, \tag{6}$$

where p is a dimensionless material parameter. Recall that $s_0 = \hat{\tau}_s(T=0)$. Equation (6) reduces to the usual Voce law
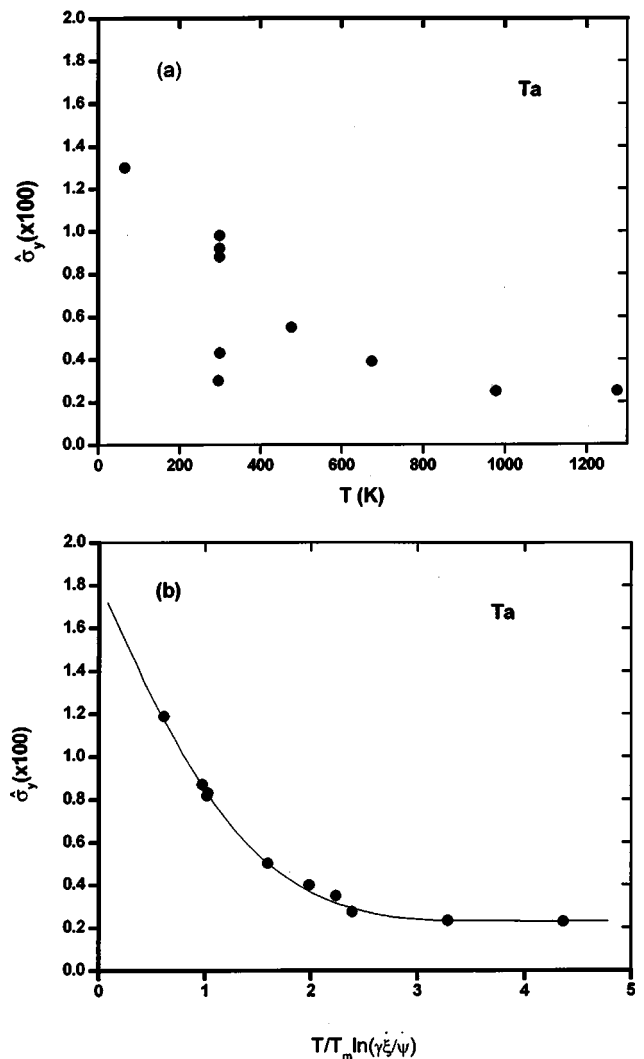

FIG. 1. Tantalum yield stress data vs (a) T and (b) $\hat{T} \ln(\gamma \dot{\xi}/\dot{\psi})$. The curve in (b) is our model. In this and subsequent figures $\sigma = 2\tau$.

when $p \to 0$. Integrating Eq. (6) along a constant strain rate path, i.e., keeping $\hat{\tau}_s$ and $\hat{\tau}_y$ constant, we find

$$\hat{\tau} = \hat{\tau}_s + \frac{1}{p}(s_0 - \hat{\tau}_y)\ln\left[1 - \left[1 - \exp\left(-p\frac{\hat{\tau}_s - \hat{\tau}_y}{s_0 - \hat{\tau}_y}\right)\right]\right.$$
$$\left. \times \exp\left\{-\frac{p\theta\psi}{(s_0 - \hat{\tau}_y)\left[\exp\left(p\dfrac{\hat{\tau}_s - \hat{\tau}_y}{s_0 - \hat{\tau}_y}\right) - 1\right]}\right\}\right]. \tag{7}$$

Equations (4) and (7) constitute our model in the thermal activation regime.

We fit our model in the thermal activation regime to low rate and Hopkinson-bar data on six pure metals and two stainless steels, namely Cu, U, Ta, Mo, V, Be, 304 SS, and 21-6-9 SS. These materials were chosen on the basis of both data availability and programmatic needs at Los Alamos National Laboratory.

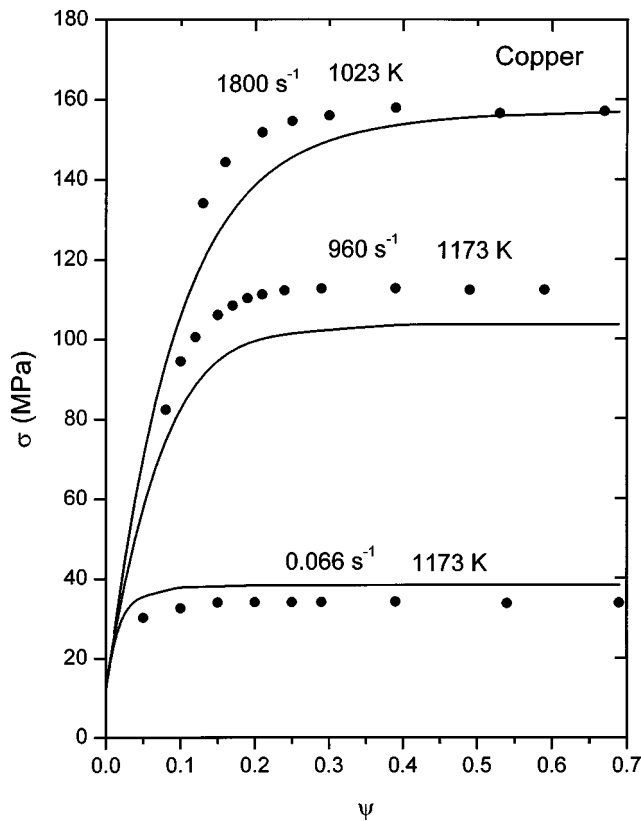We now discuss the data and model fits for each of these materials.

FIG. 2. Comparison of our model (solid curves) to the high-temperature stress–strain data of Samanta (Ref. 11).

FIG. 4. Comparison of our model (solid curves) to uranium Hopkinson-bar data of Armstrong and Wright (Ref. 12).

A. Copper

Model parameters for copper in the thermally activated regime were determined by fitting to several sources of data: room-temperature data to $\psi \approx 0.2$ at strain rates $10^{-3} - 10^{4}$ s^{-1},[10] large-strain liquid-nitrogen data (77 K) at 10^{-3} s^{-1},[4] and elevated-temperature large-strain data covering strain rates from 0.066 to 2300 s^{-1}.[11] Representative comparisons of the model to high-and low-temperature copper data are made in Figs. 2 and 3. Agreement is at the 10%
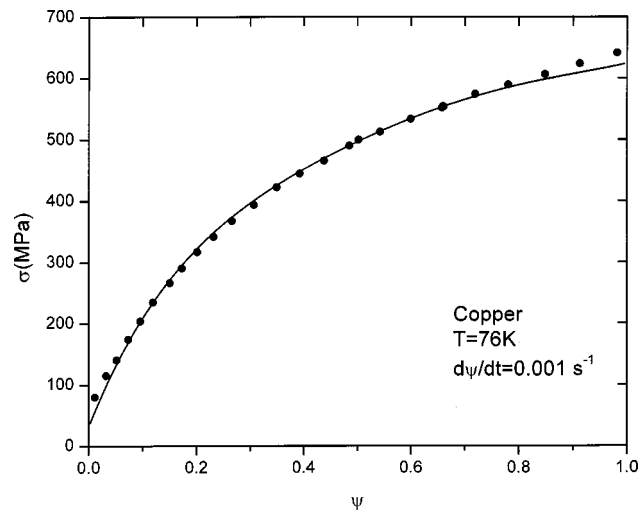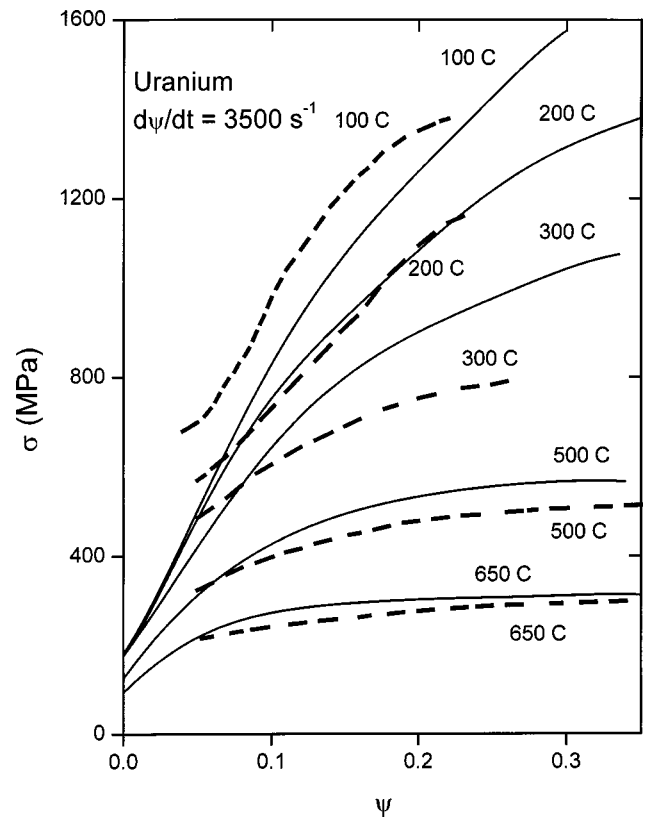
level. See Fig. 10 for a comparison of the model to room-temperature copper flow-stress data versus strain rate.

B. Uranium

Two sources of uranium data were used for the model fit. Hopkinson bar data at 3500 s^{-1} were obtained by Armstrong and Wright[12] over the temperature range $-60-900\,°C$. The samples were prepared at Los Alamos from 99.96% pure depleted uranium by means of multiple-step thermomechanical processing to produce a fine-grained ($10-40\ \mu$) isotropic microstructure. Their data and our model fit are shown in Fig. 4. Although agreement is generally 10% accurate, there is a significant, and as yet unexplained, discrepancy between the model and the data at 300 °C. The same material was tested[13] at strain rates $10^{-4} - 10^{-1}$ s^{-1} from 20 to 300 K. We did not include the 20 K data in our model fit because of anomalous behavior—increasing flow stress with decreasing strain rate—and sample cracking.

C. Tantalum, molybdenum, and vanadium

Model parameters for these bcc metals were determined from stress–strain curves[4] of commercial-purity annealed material. Tantalum strain rates ranged from 10^{-3} to 4000 s^{-1}, and temperatures varied from 77 to 1273 K. Our tantalum model is compared to Hopkinson-bar data in Fig. 5. The vanadium stress–strain data were very limited in temperature and strain rate: 77 K at 10^{-3} s^{-1}, and room-temperature data at 10^{-3}, 10^{-1}, and 6000 s^{-1}. The molybdenum data were similarly limited: 77 K at 10^{-3} and 2000 s^{-1}, and 298
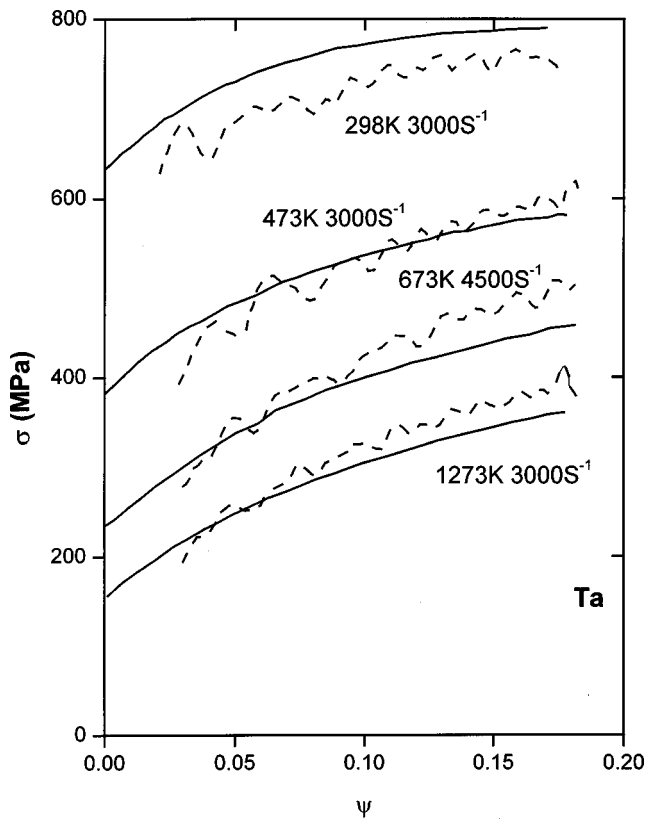

FIG. 3. Low-temperature low-rate copper data of Follansbee (Ref. 10) compared to our model (solid curve).

FIG. 5. Our model (solid curves) vs tantalum Hopkinson-bar data of Gray (Ref. 4).

FIG. 6. Comparison of our model (solid curves) to Montoya's 300 °C beryllium data (Ref. 14).

K at 10^{-3}, 10^{-1}, and 5000 s^{-1}. Fits for all three bcc metals were 10% accurate. All stress–strain data were restricted to about 20% plastic strain; hence the bcc model parameters may not be optimal for large-deformation problems.

D. Beryllium

Model parameters were determined by fitting to stress–strain data on SF200 beryllium.[14] The data set is comprehensive: at each of the four temperatures 20, 100, 200, and 300 °C there are stress–strain curves at 2×10^{-4}, 2×10^{-2}, and 2 s^{-1} to strains of 25%–30%, and two or three curves at strain rates of order 10^{3} s^{-1} to strains of roughly 15%. Our model is compared to the 300 °C data in Fig. 6. The model fits the data to comparable accuracy, namely 10%, at all three lower temperatures.

E. Stainless steels

Material parameters for 304 SS were determined by fitting to adiabatic stress–strain curves at 6000 s^{-1} at initial temperatures of 25, 200, 400, 600, and 900 °C,[15] and 304 L stress–strain data at strain rates 2×10^{-4}, 0.02, 1, 100, and 8000 s^{-1} all initially at room temperature.[4] The temperature increase along the stress–strain curves was calculated. Model agreement with all stress–strain curves was 15% or better.

Parameters for 21-6-9 SS (Nitronic 40) were fixed by fitting to the following stress–strain data: 5000 s^{-1} at 298 K, 4000 s^{-1} at 873 K, and 2000 s^{-1} at 1173 K;[15] 2×10^{-4}, 0.02,
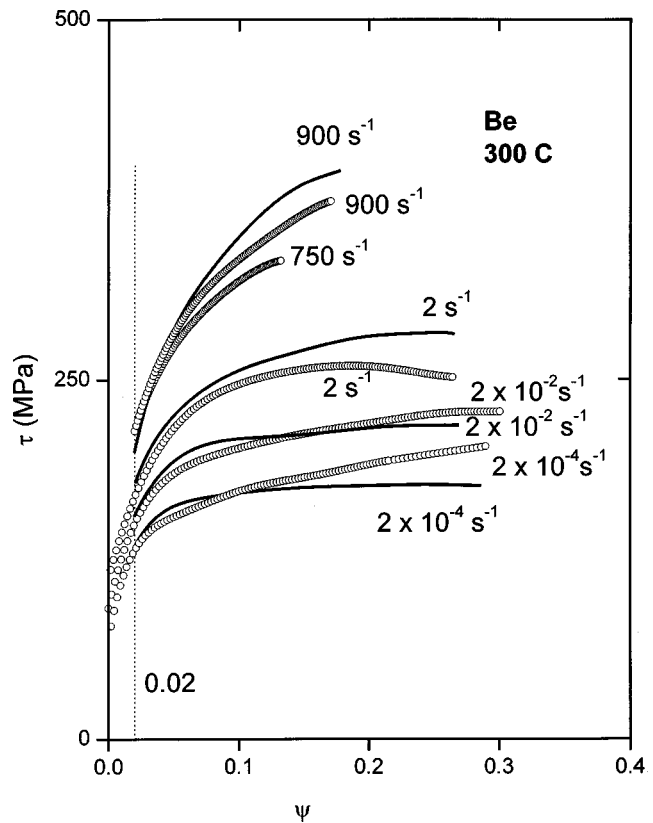
10, 100, and 5000 s^{-1} all initially at room temperature.[3] Again, the adiabatic heating was taken into account. We could not find the melting temperature of 21-6-9 SS in the literature, but because there is little variation in the melting temperatures of austenitic stainless steels, we used the 304 SS value, viz. $T_m = 1700$ K, for Nitronic 40. Similarly, the temperature dependence of the shear modulus of 21-6-9 has not been measured, so the 304 SS shear modulus was used to approximate that of 21-6-9 SS. Predicted stress–strain curves are accurate to 15%.

V. OVERDRIVEN-SHOCK REGIME

The constitutive behavior of metals in strong shock waves at plastic strain rates from 10^{9} to 10^{12} s^{-1} can be determined from Hugoniot data using Wallace's theory of overdriven shocks in metals.[16] By definition, an overdriven shock wave is one in which the plastic wave has overrun the elastic precursor to produce a front steeper than that attainable by adiabatic elastic compression. Since plastic flow only slows the shock rise,[16] heat transport to the leading edge of the shock must be present to steepen the shock front. The heat is generated by plastic flow in the latter part of the wave. Thus, an overdriven shock is comprised of two regions: a leading conduction front where heat transport occurs but plastic flow is negligible, and a plastic flow region that provides heat to the conduction front. In Wallace's scheme,[16,17] an estimate of the average deviatoric stress is obtained through the heating effect of plastic work.

In the following, we give only a brief sketch of our calculations. More detail and derivations can be found in Refs. 16 and 17 or in a document available from the authors.

Ambient values of the (assumed) constant G/B ratio, where B is the bulk modulus, were used to calculate the temperature in the conduction front, which is near ambient. The density dependence of k, the thermal conductivity, was taken into account by setting k equal to twice the high-temperature value at normal density.[16]

The shock-path calculations require T and the entropy, S, on the Hugoniot and the adiabatic bulk modulus on and off the Hugoniot. These were calculated using well known equations of McQueen et al.,[18] the assumption that the product of the density and the Grueneisen gamma is a constant, and the linear shock wave "equation of state," $D = c + s\nu$, where D is the shock velocity, ν is the particle velocity, and c and s are constants.

A set of Rayleigh-line equations is used to estimate the plastic flow and deviatoric stress in the shock as a function of the compression, ε. The temperature and heat current, J, are first calculated for the conduction front where the material is taken to be a nonplastic solid, i.e., an elastic solid that transports heat and has infinite yield strength. Differential equations for $T(\varepsilon)$ and $J(\varepsilon)$ are obtained from Eqs. (32), (33), and (34) of Ref. 16. These equations are integrated up to the point ε_C where the tangent to the $T(\varepsilon)$ curve passes through the point (ε_H, T_H) on the Hugoniot. The plastic flow region begins at the point ε_C. The path $T(\varepsilon)$ in the flow region is approximated as the line from (ε_C, T_C) to (ε_H, T_H). $T(\varepsilon)$ is closely bounded in the flow region.[17] Equation (4) in Ref. 17 is used for the increment of plastic strain. The increment of entropy, necessary to estimate the deviatoric stress, is taken from Eq. (3) of Ref. 17 with the straight-line approximation used to convert from dT to $d\varepsilon$.

When the flow-region calculation is finished, the average flow stress can be evaluated from $\langle\tau\rangle = (J_C/\rho_a D + \int_C^H T dS)/(V_C + V_H)\psi_H$, which is Eq. (7) of Ref. 17 with the entropy generated up to point C expressed in terms of the heat current.

The plastic strain rate can be estimated as explained in Sec. II E of Ref. 17 using Eq. (36) of Ref. 16. The essentials are as follows. The equations of steady wave motion can be used to relate the plastic strain rate in the shock wave to a spatial derivative of the plastic strain. The spatial differential can be written in terms of the heat flux and the temperature differential [see Eq. (36) of Ref. 16], which can then be expressed in terms of the differential in ε using the straight line path in $T-\varepsilon$. The plastic strain differential is given in terms of $d\varepsilon$ by Eq. (4) of Ref. 17. The heat flux is obtained from the following approximate entropy equation: $dJ/\rho_a D \approx T dS - (V_C + V_H)\langle\tau\rangle d\psi$.

The approximate plastic strain rate obtained along the shock path from the above equations can be averaged numerically to obtain a mean strain rate. Two numerically close versions of the mean plastic strain rate, $\langle\dot\psi\rangle_\psi$ and $\langle\dot\psi\rangle_\varepsilon$, were calculated using ψ and ε as weighting factors. A third rough estimate of the average plastic strain rate is $\langle\dot\psi\rangle_0 = [DJ_C/2k(dT/d\varepsilon)_C][(1-\varepsilon_H)/(\varepsilon_H-\varepsilon_C)]\psi_H$, which is an
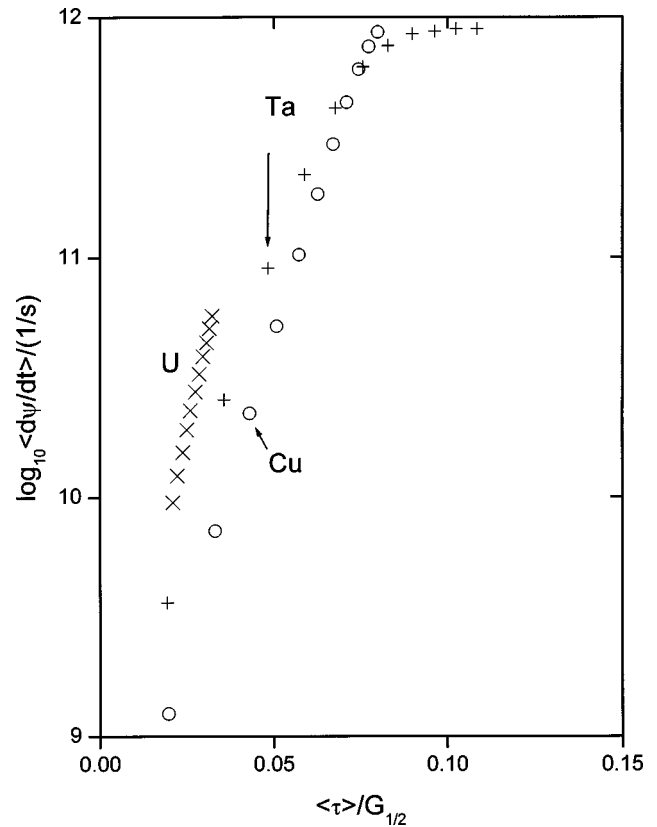

FIG. 7. Average plastic strain rate vs average deviatoric stress scaled by the shear modulus for several shock waves for three metals. The circles, pulses, and X's correspond to Cu, Ta, and U, respectively.

approximation to $\int_C^H \dot\psi d\varepsilon/(\varepsilon_H-\varepsilon_C)$. It agrees well with the other two estimates except at low pressures; See Fig. 8. It shows that, generally, $\dot\psi \sim k^{-1}$, i.e. k controls the rate of the shock process. We expect accuracy in our calculated mean strain rate only to a factor of 3, since it depends strongly on the steady-wave assumption, and on the value of the thermal conductivity.

Los Alamos internal report[19] gives details of the results of the strong shock calculations; here, we provide only a summary. Figure 7 shows the average plastic strain rate $\langle\dot\psi\rangle_\psi$ versus the scaled average deviatoric stress $\langle\tau\rangle/G_{1/2}$ for several shock strengths for Cu, Ta, and U. $G_{1/2}$ is the value of the shear modulus at the point along the shock path where one-half of the final plastic strain is attained. Preliminary calculations showed that this value differs from the average through the plastic flow region by only a few percent. The results for $\langle\dot\psi\rangle_\varepsilon$ were almost the same as for $\langle\dot\psi\rangle_\psi$. Figure 8 shows these quantities for copper on a log–log plot to demonstrate the approximate power-law dependence of strain rate on scaled deviatoric stress. Lower strain rate data from the pressure-shear gas gun experiments[20] also shown are consistent with the overall power-law dependence. The three sets of symbols for the strong shock results correspond to the three different averages, which produce similar results.

Figures 7 and 8 clearly show, with the exception of Ta near 10^{12} s^{-1}, that for the strong shock path, the mean flow stress scaled by the shear modulus has a power-law dependence on the plastic strain rate. For the high temperatures
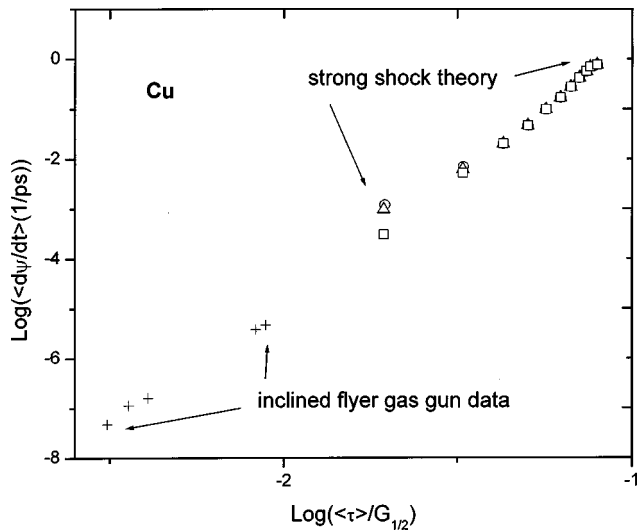
FIG. 8. Average plastic strain rate vs average deviatoric stress divided by the shear modulus for Cu. The five pluses are pressure-shear gas gun data of Huang and Clifton (Ref. 20). The squares, triangles, and circles correspond to three different averaging schemes for the plastic strain rate along the shock path: a rough average, volumetric-strain weighting, and plastic-strain weighting.
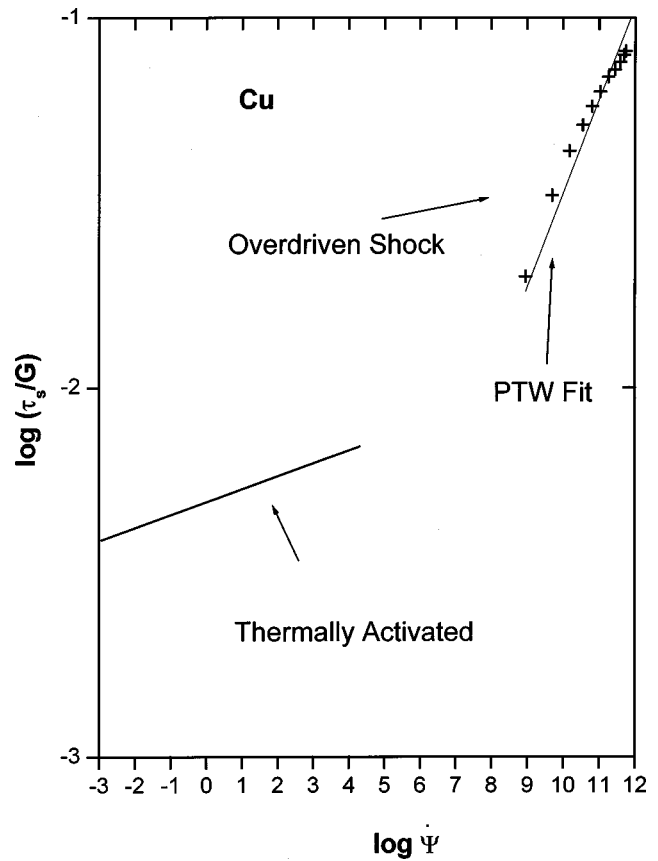

FIG. 9. Copper saturation stress in the thermal-activation regime and overdriven-shock results with our model fit to those results. The rate sensitivity is much higher at strong-shock rates than at Hopkinson-bar strain rates and below.

and large strains of the strong shock path, the work hardening is probably saturated. We, therefore, neglect work hardening (no ψ dependence) at these very high strain rates and model the saturation and yield stresses in the overdriven shock regime, namely $10^9 - 10^{12}$ s^{-1}, as

$$\hat{\tau}_s = \hat{\tau}_y = \text{constant} \times (\dot{\psi}/\dot{\xi})^\beta, \qquad (8)$$

where the exponent β was determined to be 0.25, 0.23, and 0.27 for Cu, Ta, and U, respectively. We consider strong-shock analyses for additional materials unnecessary for our constitutive model because the variation in β for Cu, Ta, and U is only a few percent. The Cu (fcc) value, $\beta = 0.25$, is used in our model for the fcc stainless steels, and β is taken to be 0.23, the Ta (bcc) value, for the bcc metals V and Mo. The mean value of β, namely 0.25, is used for Be.

The sensitivity of the results to the values of G/B and γ_a (Grueneisen) was assessed by varying them about the standard values in Table I. In general, changing G/B and γ_a by 10% produced a similar or smaller variation in $\langle\tau\rangle/G_{1/2}$ and a variation in $\log\langle\dot{\psi}\rangle_\varepsilon$ of a few percent.

TABLE I. Material parameters used in strong shock calculations (see Refs. 16, 17, and 19 for the parameter definitions).

	Cu	U	Ta
M (m_u)	63.54	238.04	180.948
c (cm/μs)	0.3933	0.2487	0.3293
s	1.50	2.20	1.307
ρ_a (g/cm^3)	8.933	19.07	16.75
γ_a	2.0	2.1	1.7
G/B	0.35	0.75	0.36
ρ_0 (g/cm^3)	9.02	19.2	16.8
$\Gamma(\rho_0)(10^{-4}$ cal/mol K^2)	1.6	12.4	6.8
g	2/3	7/3	5/3
k (cal/s cm K)	1.8	0.2	0.3

We briefly discuss the basic physical assumptions and validity of the strong shock theory. A typical shock thickness and rise time for a Mbar shock is 100 Å and 2 ps. The former is large enough to justify a continuum description while the latter is almost as small as a phonon vibration frequency and is borderline.[17] Nevertheless, considerations of relaxation times and mean free paths of phonons and electrons indicate that irreversible thermodynamics is valid for shocks up to a few Mbar.[17] Our high-strain-rate model is based on the strong-shock loading path. Valid applications of the high-strain-rate part of our model are limited to high pressures and high temperatures near this path. Appropriate applications include high-velocity impact and high-explosive-driven deformation. Davidson and Walsh[21] successfully used the high-strain-rate portion of our model to simulate high-velocity impact cratering. The power-law form has been found by Holian *et al.*[22] to fit molecular dynamics shock-wave simulations.

VI. TRANSITION FROM THERMALLY ACTIVATED GLIDE TO THE OVERDRIVEN SHOCK REGIME

Figure 9 contrasts the 300 K thermally assisted saturation stress (this model) up to 10^4 s^{-1} (thermal activation may be rate controlling up to higher rates) with the results of the overdriven shock calculations (crosses) and our power-law fit to those results. There is a five-decade gap separating
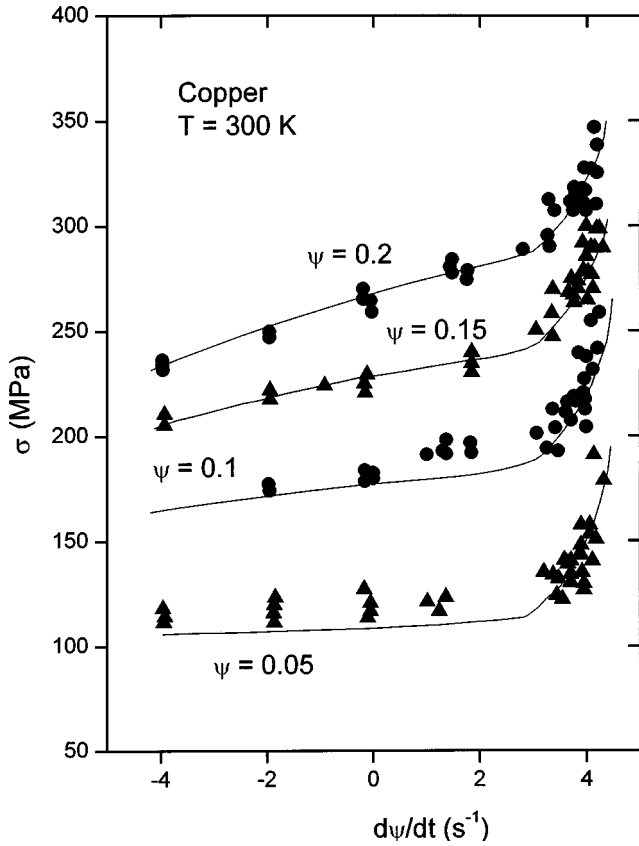
FIG. 10. Our model (solid curves) compared to Follansbee's room-temperature constant-strain stress–strain-rate data on copper.

them. A significant increase in the rate sensitivity occurs in the gap; errors in the shock calculations and low rate model are far too small to invalidate this conclusion. In the absence of validated experimental data[23] or an established theory of deformation at these intermediate strain rates, we model the gap in the simplest way possible and without introducing any additional material parameters, the saturation stress is the greater of $\hat{\tau}_s$ as given by Eq. (4) or the power law Eq. (8) with the constant coefficient set equal to $s_0 \gamma^{-\beta}$ in order to maintain continuity of the stress:

$$\hat{\tau}_s = \max\{s_0 - (s_0 - s_\infty)\mathrm{erf}[\kappa \hat{T} \ln(\gamma \dot{\xi}/\dot{\psi})], \ s_0(\dot{\psi}/\gamma\dot{\xi})^\beta\}. \tag{9}$$

An abrupt increase in the constant-strain rate sensitivity at small plastic strains is well known.[24] Figure 10, Follansbee's[10] room-temperature constant-strain stress–strain-rate copper data, is a good example. A jump in rate sensitivity at about 10^3 s^{-1} is evident. The rate sensitivity actually exceeds that calculated from overdriven shock theory for rates above 10^9 s^{-1}. Similar behavior is expected for other metals. Our expression for $\hat{\tau}_y$ is similar to Eq. (9) but includes two additional parameters, y_1 and y_2, to allow for such a maximum in the small-strain rate sensitivity:

$$\hat{\tau}_y = \max\{y_0 - (y_0 - y_\infty)\mathrm{erf}[\kappa \hat{T} \ln(\gamma \dot{\xi}/\dot{\psi})],$$
$$\min[y_1(\dot{\psi}/\gamma\dot{\xi})^{y_2}, s_0(\dot{\psi}/\gamma\dot{\xi})^\beta]\}. \tag{10}$$

With this expression for $\hat{\tau}_y$, our copper model accurately accounts for the jump in rate sensitivity at 10^3 s^{-1}, as well as an increase in rate sensitivity with strain at rates under 10^3 s^{-1}: See Fig. 10.

For some metals, uranium for example, the behavior at intermediate strain rates is modeled as an extrapolation of the overdriven shock results, hence $y_1 = s_0$ and $y_2 = \beta$. In this case, the transition can be smoothed without introducing any additional parameters by simply adding the error function and power-law terms. This modification has been observed to slightly improve calculated Taylor impact cylinder lengths.[25]

Some recent references on the broader issue of transition in mechanism at high plastic strain rate are Refs. 26–28.

VII. SHEAR MODULUS AND MELTING TEMPERATURE

Our plastic constitutive relation, comprised of Eqs. (7), (9), and (10), requires models for the adiabatic shear modulus, $G(\rho,T)$, and the melting temperature, $T_m(\rho)$. It is critical that accurate representations of $G(\rho,T)$ and $T_m(\rho)$ are used for explosive loading simulations where extremes of temperature and density are involved.

The temperature dependence of $G(\rho,T)$ involves two temperature scales: the melting temperature and a characteristic temperature, typically a few tens of degrees Kelvin, below which G is strongly nonlinear in T. A good model[29] of $G(\rho,T)$ is realized by ignoring the low-temperature nonlinearity and approximating $G(\rho,T)$ as a linear function of the scaled temperature $\hat{T}(\rho) = T/T_m(\rho)$:

$$G(\rho,T) = G_0(\rho)(1 - \alpha\hat{T}). \tag{11}$$

The parameter α is expected to be a function of the density, but because the ρ dependence is not known for any material, we simply take it to be a constant. Its value is determined from zero-pressure data after correcting to constant density. The thermodynamic data needed to determine α are available for Cu and U, but not for Ta, V, Mo, Be, 304 SS, or 21-6-9 SS. Consequently, we assign the mean value of α for sixteen metals,[29] namely 0.23, to those six materials.

It is sometimes convenient to work with pressure, P, rather than ρ. In that case we simply make the replacements $\rho \rightarrow P$ and $\alpha \rightarrow \alpha_P$ in Eq. (11). The values of the constant-pressure thermal softening parameter, α_P, for Cu, U, Ta, Mo, 304 SS, and 21-6-9 SS are provided in Table II. Values of α_P for Be and V cannot be determined because the zero-pressure shear-modulus data on these elements are limited to temperatures of only $0.19T_m$ and $0.14T_m$, respectively.

$G_0(\rho)$ can be estimated by employing simple analytic forms to extrapolate from ambient conditions using the measured values of the shear modulus and its first pressure derivative[2,30] or the results of first-principles electronic structure calculations.[30,31] When $G_0(\rho)$ is required over extremes in pressure, say zero to tens of megabars, then it is most accurately estimated by combining Eq. (11) with the Burakovsky–Preston melting relation[7] with the result that $G_0(\rho) = \mathrm{constant} \times \rho T_m(\rho)/(1 - \alpha)$.

All three scaling variables in our model depend on $T_m(\rho)$; for α constant, the density dependencies of the scaling variables for τ, T, and $\dot{\psi}$ are, respectively, $\rho T_m(\rho)$,

TABLE II. Model material parameters; G_0 entries are in kilobars.

	Cu	U	Ta	V	Mo	Be	304 SS	21-6-9 SS
θ	0.025	0.055	0.02	0.023	0.014	0.04	0.02	0.02
p	2.0	1.0	0.0	0.0	0.0	1.4	10.0	8.0
s_0	0.0085	0.03	0.012	0.013	0.009 45	0.007	0.05	0.05
s_∞	0.000 55	0.0015	0.003 25	0.004 05	0.0038	0.0012	0.0075	0.0075
κ	0.11	0.13	0.6	0.4	0.41	0.14	0.3	0.3
γ	0.000 01	0.002	0.000 04	0.000 06	0.000 008	0.000 01	0.001	0.001
y_0	0.0001	0.000 75	0.01	0.0105	0.007 95	0.0015	0.0069	0.0125
y_∞	0.0001	0.000 75	0.001 25	0.001 55	0.0023	0.0005	0.0015	0.002 25
y_1	0.094	0.03	0.012	0.013	0.009 45	0.007	0.05	0.05
y_2	0.575	0.27	0.4	0.42	0.36	0.25	0.46	0.41
β	0.25	0.27	0.23	0.23	0.23	0.25	0.25	0.25
G_0	518	938	722	499	1303	1524	895	862
α	0.20	0.56	0.23	0.23	0.23	0.23	0.23	0.23
α_p	0.43	0.72	0.48		0.41		0.66	0.37

$T_m(\rho)$, and $\rho^{1/3}T_m^{1/2}(\rho)$. At modest densities, $T_m(\rho)$ is best obtained from the measured $T_m(P)$, while the high compression behavior is most reliably estimated by extrapolating from the low-pressure data by means of the Lindemann criterion.

VIII. COMPLETE MODEL

Values of the model parameters for our set of six metals and two stainless steels are given in Table II. Note that the order of magnitude of a given parameter is usually independent of the metal. The plastic constitutive parameter values are strikingly similar among the bcc metals Ta, Mo, and V. This regularity in the parameter values gives us a predictive capability even in the absence of data, and suggests that our model is based on the correct physics.

The global structure of our model, i.e., the thermal activation and very-high-rate regimes, plus the transition region connecting them, is depicted for copper, a generic example in Fig. 11. Several features are noteworthy. In the thermal-activation regime, the rate sensitivity of the saturation stress is nearly constant at room temperature and below but increases with strain rate as $T \rightarrow T_m$. Saturation and yield

stresses merge continuously into the very-high-rate power-law as $\dot\psi \rightarrow \gamma\dot\xi$. There is a weak temperature dependence at very high rates that may be described as "thermal hardening."

IX. COMPARISON TO PRESSURE-SHEAR GAS GUN DATA

Stress–strain data at strain rates much higher than 10^4 s^{-1} (Hopkinson bar data) are rare, but data on copper and tantalum at strain rates up to $10^6/$s^{-1} are now available. The data were recently obtained by Clifton et al.[32,37] from pressure-shear gas gun experiments.

In Table III we compare the peak experimental von Mises flow stresses to the model values for six pressure-shear experiments on OFHC copper.[32] The experimental loading path was approximated as follows. The calculated sample densities after impact but before shearing were taken to be the shock Hugoniot densities at the experimental values of the pressure;[32] the dependence of the preshot density on the preshot temperature of the heated samples was included in the calculation of the Hugoniot density. For each sample at its calculated pressurized but preshear density, $T_m(\rho)$ was obtained using the Lindemann melting criterion, and the pressurized but unsheared sample temperature was estimated as the Hugoniot temperature for a Mie–Grueneisen equation of state. Adiabatic heating of the samples during shearing was calculated assuming that 90% of the plastic work is dissipated. The pressure dependence of G is very nearly linear
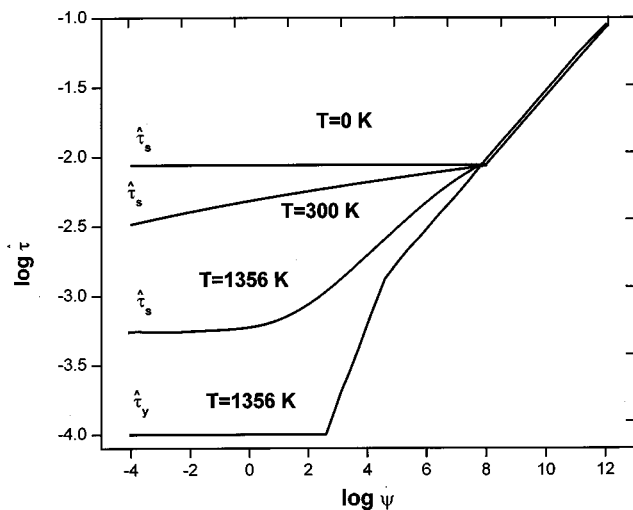

FIG. 11. Global structure of our copper model.

TABLE III. Comparison of peak experimental von Mises flow stress, $\sigma_{\text{data}}(\psi_{\text{peak}})$, to calculated values, $\sigma_{\text{model}}(\psi_{\text{peak}})$, for six pressure-shear experiments on OFHC copper (Ref. 32). The initial sample temperature is T_0. The strains are von Mises equivalent strains.

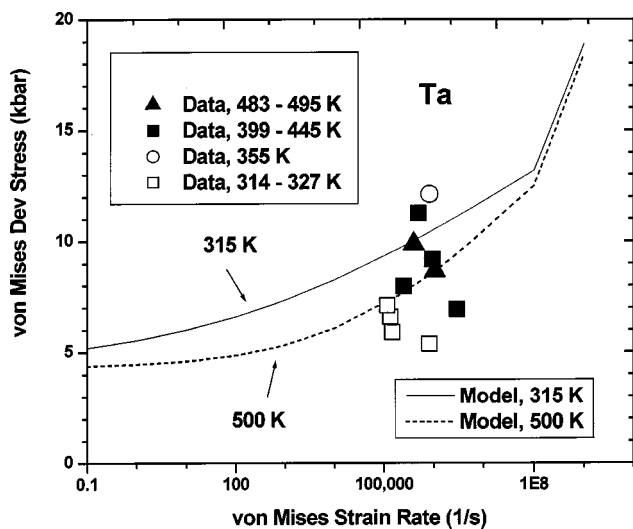| Expt.	T_0 (K)	P (GPa)	$\dot\psi$ (μs^{-1})	ψ_{peak}	σ_{data} (MPa)	σ_{model} (MPa)
a	571	7.8	0.13	0.12	589	391
b	768	7.4	0.15	0.14	485	381
c	964	7.8	0.14	0.12	485	329
A	571	8.0	0.64	0.23	866	562
B	768	7.7	0.64	0.23	762	511
C	964	7.8	0.81	0.46	624	517

FIG. 12. Model flow stresses for tantalum at two temperatures versus pressure-shear gas gun data. The data temperature ranges are calculated from adiabatic heating due to plastic work.

up to the maximum sample pressures (~80 kbar), hence it was calculated using $(\partial G/\partial P)_{P=0}=1.36$, and the thermal softening of G was calculated using $\alpha_P=0.43$. As seen in Table III, the experimental values of the flow stress are consistently higher than the calculated values: the model values vary from 17% to 35% too low.

For case B in Table III (shot KF 9609), our model prediction is 33% too low. For comparison, using Fig. 10 of Ref. 32, the Follansbee and Kocks with Johnson and Tonks[33,34] model prediction at the peak experimental stress is 43% too low, the Zerelli and Armstrong[35] model prediction is 60% too low, and the Johnson and Cook[36] prediction is 71% too low.

Duprey and Clifton[37] measured pressure shear data for tantalum at ambient initial conditions. The peak experimental stresses are compared to the predictions of our model in Fig. 12. For shots KD9401 and KD9704, however, data points at shear strains of 0.1 and 0.5 were used instead of peak points because no clear peaks are evident. Total adiabatic conversion of plastic work into heat was assumed to obtain the final experimental temperatures. Effects of the initial shock pressurization of about 45 kbar and the plastic adiabatic heating are small—the density changes by only about 2% and are ignored in the calculation. Our model roughly agrees with the data, but great scatter is evident in the data. The authors[37] originally attributed the scatter to texture effects, but they subsequently performed numerical simulations that ruled out this explanation for the scatter.[38]

[1] G. R. Johnson and W. H. Cook, in Proceedings of Seventh International Symposium on Ballistics, The Hague, The Netherlands, April, 1983; F. J. Zerilli and R. W. Armstrong, J. Appl. Phys. **61**, 1816 (1987).

[2] D. J. Steinberg, S. G. Cochran, and M. W. Guinan, J. Appl. Phys. **51**, 1498 (1980).

[3] P. S. Follansbee and U. F. Kocks, Acta Metall. **36**, 81 (1988).

[4] G. T. Gray III (private communication).

[5] G. I. Taylor, Proc. R. Soc. London, Ser. A **145**, 362 (1934).

[6] F. A. Lindemann, Z. Phys. **11**, 609 (1910).

[7] L. Burakovsky and D. L. Preston, Solid State Commun. **115**, 341 (2000); L. Burakovsky, D. L. Preston, and R. R. Silbar, Phys. Rev. B **61**, 15011 (2000); J. Appl. Phys. **88**, 6294 (2000).

[8] S. Glasstone, K. J. Laidler, and H. Eyring, *The Theory of Rate Processes* (McGraw-Hill, New York, 1941); G. H. Vineyard, J. Phys. Chem. Solids **3**, 121 (1957); N. B. Slater, *Theory of Unimolecular Reactions* (Cornell University Press, Ithaca, NY, 1959); S. Chandrasekhar, Rev. Mod. Phys. **15**, 1 (1943).

[9] E. Voce, J. Inst. Met. **74**, 537 (1947/48).

[10] P. S. Follansbee, Los Alamos National Laboratory Report No. LA-UR-85-3026.

[11] S. K. Samanta, J. Mech. Phys. Solids **19**, 117 (1971).

[12] P. E. Armstrong and W. J. Wright, Los Alamos National Laboratory Report No. LA-CP-85-353.

[13] J. E. Hockett, P. S. Gilman, and O. D. Sherby, J. Nucl. Mater. **64**, 231 (1977).

[14] D. Montoya, Commissariat a l'Energie Atomique Report No. CEA-R-5595, 1992.

[15] P. S. Follansbee and P. E. Armstrong, Los Alamos National Laboratory, January, 1983.

[16] D. C. Wallace, Phys. Rev. B **24**, 5597 (1981).

[17] D. C. Wallace, Phys. Rev. B **24**, 5607 (1981).

[18] R. G. McQueen, S. P. Marsh, J. W. Taylor, J. N. Fritz, and W. J. Carter, in *High-Velocity Impact Phenomena*, edited by R. Kinslow (Academic, New York, 1970), p. 293.

[19] D. L. Tonks, Los Alamos National Laboratory Report No. LA 12641, 1993.

[20] S. Huang and R. J. Clifton, in *Macro- and Micromechanics of High Velocity Deformation and Fracture*, edited by K. Kawata and J. Shiori (IUTAM, Tokyo, 1985), p. 63.

[21] R. F. Davidson and M. L. Walsh, AIP Conf. Proc. **370**, 1159 (1996).

[22] B. L. Holian, J. E. Hammerberg, and P. S. Lomdahl, J. Comput.-Aided Mater. Des. **5**, 207 (1998).

[23] Pressure-shear impact technique (Ref. 20) provides strength data at strain rates from 10^5 to 10^7 s^{-1}, but interpretation of the data is still open to question.

[24] A. Kumar and R. G. Kumble, J. Appl. Phys. **40**, 3475 (1969); J. W. Eddington, Philos. Mag. **19**, 1189 (1969); F. E. Hauser, J. A. Simmons, and J. E. Dorn, in *Response of Metals to High Velocity Deformations*, edited by P. G. Shewmon and V. F. Zackary (Interscience, New York, 1961), p. 93; D. L. Davidson, U. S. Lindholm, and L. M. Yeakley, Acta. Metall. **14**, 703 (1966).

[25] P. Elias and N. Moulin (private communication).

[26] K. E. Duprey and R. J. Clifton, in *Shock Compression of Condensed Matter-1997*, edited by S. C. Schmidt, D. P. Dandekar, and J. W. Forbes (AIP, Woodbury, New York, 1998), p. 475.

[27] J. N. Johnson, in *High Pressure Science and Technology-1993*, edited by S. C. Schmidt, J. W. Shaner, G. A. Samara, and M. Ross (AIP, Woodbury, New York, 1994), p. 1145.

[28] H. Zbib, M. Hiratani, and M. A. Khaleel, in *Plasticity, Damage, and Fracture at Macro, Micro and Nano Scales*, edited by A. S. Khan and O. Lopez-Pamies (Neat, Fulton, MD, 2002), p. 99.

[29] D. L. Preston and D. C. Wallace, Solid State Commun. **81**, 277 (1992).

[30] G. K. Straub, Los Alamos National Laboratory Report No. LA-11806-MS, 1990.

[31] P. Soderlind and J. Moriarty, Phys. Rev. B **57**, 10340 (1998).

[32] K. J. Frutschy and R. J. Clifton, J. Mech. Phys. Solids **46**, 1723 (1998).

[33] P. S. Follansbee and U. F. Kocks, Acta. Metall. **36**, 81 (1988).

[34] J. N. Johnson and D. L. Tonks, in *Shock Compression of Condensed Matter*, edited by S. C. Schmidt, R. D. Dick, J. W. Forbes, and D. G. Tasker (Elsevier Science, New York, 1992), p. 371.

[35] F. J. Zerelli and R. W. Armstrong, J. Appl. Phys. **61**, 1816 (1987).

[36] G. R. Johnson and W. H. Cook, Eng. Fract. Mech. **21**, 31 (1985).

[37] K. E. Duprey and R. J. Clifton, in *Shock Compression of Condensed Matter*, edited by S. C. Schmidt, D. P. Dandekar, and J. W. Forbes (AIP, Woodbury, NY, 1997), p. 475.

[38] R. J. Clifton (private communication).